

# Crack propagation and coalescence due to dual non-penetrating surface flaws and their effect on the strength of rock-like material

Jun Xu<sup>1</sup>, Zheyuan Zheng<sup>1</sup>, Xiaochun Xiao<sup>2</sup> and Zhaoxia Li<sup>1,3</sup>

<sup>1</sup> Department of Engineering Mechanics, Jiangsu Key Laboratory of Engineering Mechanics, Southeast University, Nanjing 210096, People's Republic of China

<sup>2</sup> School of Mechanics & Engineering, Liaoning Technical University, Fuxin 123000, People's Republic of China

E-mail: [jxu1225@seu.edu.cn](mailto:jxu1225@seu.edu.cn), [zhy\\_zheng@seu.edu.cn](mailto:zhy_zheng@seu.edu.cn), [xxc7902@163.com](mailto:xxc7902@163.com) and [zhxli@seu.edu.cn](mailto:zhxli@seu.edu.cn)

Received 2 March 2017, revised 22 November 2017

Accepted for publication 22 January 2018

Published 13 March 2018



## Abstract

Non-penetrating surface flaws play a key role in the fracture process of rock-like material, and could cause localized collapse and even failure of the materials. Until now, the mechanism and the effect of surface crack propagation have remained unclear. In this paper, compression tests on gypsum (a soft rock material) are conducted to investigate crack propagation and coalescence due to non-penetrating surface flaws and their effect on the material strength. Specimens are tested under dual pre-existing surface flaws with various combinations of depth and spacing. The results show that when the pre-existing flaws are non-penetrating, the  $d/t$  ratio (flaw depth ratio,  $d$  is the pre-existing flaw cutting depth and  $t$  is the specimen thickness) and the spacing (the distance between the two flaw internal tips) have a strong influence on surface crack patterns and specimen strength. Few cracks emanate from the pre-existing flaws when the flaw depth ratio is equal to  $1/3$ , and more cracks occur with the increase of the flaw depth ratio. When the pre-existing flaw penetrates completely through the specimen, the spacing has a small effect on the specimen strength. A larger flaw depth ratio could advance the occurrence of the peak load (PL) and result in a smaller specimen residual strength. The failure process of the specimen is divided into several stages featured by a stepped decline of the load value after PL, which is closely related to the initiation and propagation of secondary cracks. In addition, the spalling (failure of a portion of the surface caused by coalescence of cracks) can be regarded as indicating the failure of the specimen, and two possible types of spalling formation are briefly discussed.

**Keywords:** non-penetrating surface flaw, crack propagation and coalescence, strength, flaw depth ratio, spacing

(Some figures may appear in colour only in the online journal)

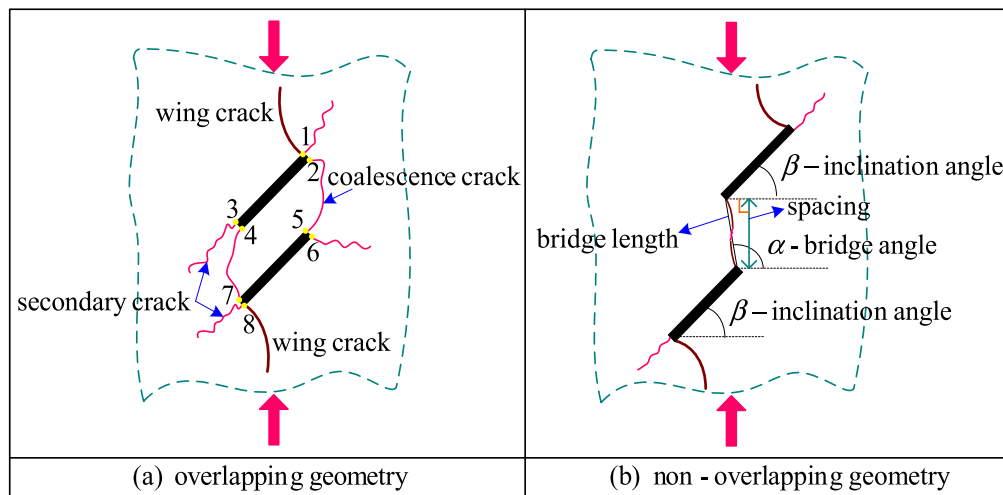
<sup>3</sup> Authors to whom any correspondence should be addressed.



Original content from this work may be used under the terms of the [Creative Commons Attribution 3.0 licence](https://creativecommons.org/licenses/by/3.0/). Any further distribution of this work must maintain attribution to the author(s) and the title of the work, journal citation and DOI.

## 1. Introduction

In geotechnical engineering, there are a significant number of natural or artificial flaws that do not always penetrate completely through the rock mass. The propagation and coalescence of these non-penetrating flaws in rocks or engineering structures play an important role in determining the mechanical and physical properties of materials. A thorough understanding of the growth, propagation, and coalescence of



**Figure 1.** Crack pattern in specimen with two parallel and overlapping or non-overlapping pre-existing flaws in uniaxial compression. Tips 3–6 are internal tips, and tips 1, 2, 7 and 8 are external tips.

three-dimensional crack networks is critical for predicting the failure of soft rock-like material. Previous studies, have investigated the initiation, propagation and coalescence of single or multiple pre-existing penetrating cracks in brittle solids under compression, and they considered different materials including glass (Brace and Bombolakis 1963, Hoek and Bieniawski 1965), polymethyl methacrylate (PMMA) (Ashby and Hallam 1986), marble (Huang *et al* 1990), granite (Li *et al* 2005, Morgen *et al* 2013), sandstone (Yang 2011, Yang and Jing 2011), limestone (Feng *et al* 2009, Yang *et al* 2013), ice (Schulson *et al* 1991) and mixed rock-type materials (Ingraffea and Heuze 1980, Wong and Chau 1998, Wong *et al* 2001, Mughieda and Alzo'ubi 2004, Zhou *et al* 2014, Haeri *et al* 2014a, 2014b, Cao *et al* 2015).

By using gypsum specimens, Lajtai (1971, 1974) found that fracture initiation greatly depends on the geometry of wing cracks, which is the term usually given to the tensile cracks that initiate at the points of maximum tensile stress concentration and propagate along a curvilinear direction that becomes roughly parallel to the far field compression, as shown in figure 1(a). In addition, secondary cracks also initiate from the flaw tips, similar to tensile crack initiation, except that the extended direction and stress level of initiation are determined by the direction and magnitude of maximum shear (Bobet 2000). A coalescence crack could be produced by a tensile crack or shear crack or mixed tensile and shear cracks (Bobet and Einstein 1998a), as shown in figure 1(a). Meanwhile, the generation of shear fractures and tension fractures could be combined, which often marks the failure of a specimen. According to the work (Reyes and Einstein 1991) on the coalescence modes of cracks, the relative positions of the pre-existing flaws play a significant role in crack coalescence. The cracks would interconnect in the propagation process if the pre-existing flaws overlap, as presented in figure 1(a). Further investigation of crack initiation, propagation and coalescence in gypsum under uniaxial and biaxial compression was carried out by Shen (1995) and Bobet and Einstein (1998a). Their results indicate that the position where

the wing crack initiates also depends on the magnitude of confining stress that transits from the flaw tip to the middle of the flaw and finally disappears with increasing confinement. The research on crack propagation and coalescence from microscopic to macroscopic scale in gypsum and Carrara marble specimens with one and two pre-existing flaws was conducted by Wong and Einstein (2009a, 2009b). They conclude that the coalescence type is related to bridge length, bridge angle and flaw inclination angle, as shown in figure 1(b). In addition, the different mechanisms of wing and secondary cracks are discussed based on the observations, which are also discussed by Haeri *et al* (2015a) via rock-like (disk) specimens.

For the coalescence of multiple flaws, Sagong and Bobet (2002) note that under uniaxial compression, the cracking pattern is analogous to the result of the specimen containing two flaws. Park and Bobet (2009, 2010) found that the initiation, propagation and coalescence of cracks from pre-existing flaws in gypsum are similar for both open and closed flaws. In addition, Haeri *et al* (2014a, 2014b, 2014c, 2015a, 2015b) also investigated the crack propagation and coalescence in rock-like (disk) specimens with random pre-existing flaws via experimental and numerical tests. In addition, many numerical simulations (Shen and Stephansson 1993, Bobet and Einstein 1998b, Tang *et al* 2001, Lee and Jeon 2011, Zhou and Yang 2012, Wong and Li 2013, Bi *et al* 2016) suggest that the flaw number, geometry, and angle of inclination with respect to the load and spacing of the flaws have certain effects on crack initiation, propagation and coalescence.

However, the aforementioned studies mainly concentrate on the pre-existing flaws that completely penetrate the (two dimensional) specimen. Less work has been done on crack growth from pre-existing flaws that do not penetrate completely through the specimen, which is a more complicated non-planar problem. Teng *et al* (1987) found that crack growth from non-penetrating flaws is spiral and not coplanar to the initial flaws. 3D wing cracks were studied by Dyskin *et al* (1999, 2003), in which the growth of wing cracks from

pre-existing flaws was influenced by their shape, location and spacing. Based on experimental observations (Wong *et al* 2004a, 2004b, 2007), for a given flaw depth and bridge length, the effect of bridge angle on the coalescence of surface cracks in granite seems similar to the effect of penetrating flaws (Yin *et al* 2014). According to the discussion about the impact of the pre-existing surface flaw geometry and the boundary on 3D surface fracture propagation (Wong *et al* 2004a, 2004b), the length of crack propagation depends heavily on the ratio of flaw depth ( $d$ ) to specimen thickness ( $t$ ), and cracks propagate easier and further as the ratio is equal to or greater than  $1/3$  (Huang and Wong 2007). A series of tests on PMMA specimens containing two parallel surface cracks under uniaxial compression show that the coalescence is mainly induced by the interaction of two wing cracks when  $d/t \geq 1/3$ , and when  $d/t < 1/3$ . The coalescence is dominantly caused by the linkage of the extensions of petal cracks (perhaps they are initiated by the concentrated shear on the plane of the crack Adams and Sines 1978). In Liang *et al* (2012), the numerically simulated results demonstrate that rock heterogeneity and inclination of the pre-existing flaw are important factors that could affect the crack patterns and peak uniaxial compressive strength of rock specimens.

To investigate the propagation and coalescence of non-penetrating surface flaws and their effect on the strength of soft rock material, gypsum was selected for the experimental investigation. It is a typical soft rock with the following advantages: (1) gypsum is an ideal weak, brittle, porous solid, and the propagation and coalescence of cracks is easy to observe, and (2) it can be moulded into different shapes flexibly and rapidly. Therefore, Vekinis *et al* (1993) suggest that gypsum is suitable for the study of rocks, cement and ceramics in tests. Many relevant experimental results so far have been accumulated.

## 2. Experimental observations on crack propagation and coalescence

### 2.1. Description of the specimen and the test

Gypsum specimens used in the test are made of gypsum powder and water, mixed with a ratio of 225:100, and the mould is shown in figure 2(a). The dimension of the specimen is 70 mm  $\times$  140 mm  $\times$  30 mm (width  $\times$  height  $\times$  thickness), and main geometric parameters of the specimen, including flaw length ( $2a$ ), inclination angle ( $\beta = 45^\circ$ ) and spacing ( $S$ ), are shown in figure 2(b). It should be noted that the spacing in this paper is the vertical distance between the two internal tips (tips 4 and 5 in figure 1(a)) of the pre-existing flaws in the axial direction of the specimen. The pre-existing flaws are produced by the sheet metal, as shown in figure 2(a). In addition, the two pre-existing flaws are all open flaws that are parallel and overlapping with each other. Different distances between the two pre-existing flaw tips of 0, 10, 20, 30 and 40 mm were used in the test. Meanwhile, three values for the ratios of flaw depth ( $d$ ) to thickness ( $t$ ) were

used, which are  $1/3$ ,  $2/3$  and  $1$ , respectively, as shown in figure 2(c).

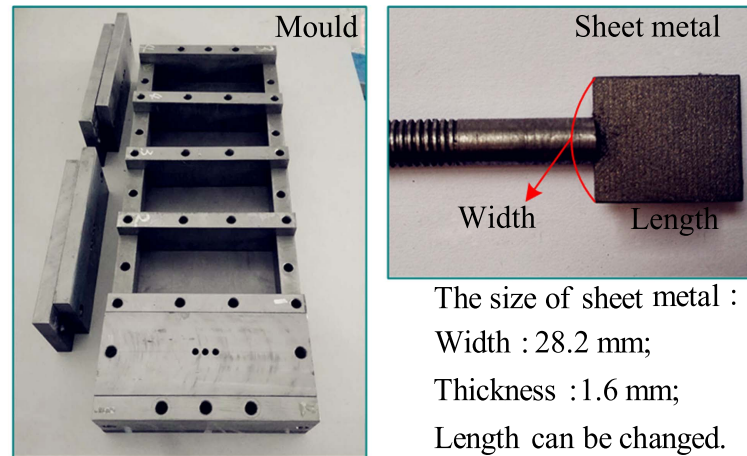
Furthermore, in the preparation process, the gypsum specimens taken out of the mould are put in the thermostat for approximately 10 d. The specimens are loaded uniaxially in compression by the testing machine of the Mechanical Testing and Simulation system (600 kN) at a shortening rate of  $0.002 \text{ mm s}^{-1}$ , which is a suggested rate to ensure a static loading condition from the experimental study on gypsum by Bobet and Einstein (1998a). The loading system does not only control the loading mode but also records the force and displacement during the experimental period. Moreover, a High Definition (HD) camera is utilized to detect and record the patterns of crack propagation and coalescence from the surfaces of the specimens. More detailed experimental instruments and equipment are presented in figure 3, and the various combinations of flaw depth and flaw spacing are listed in table 1 where the # symbol refers to the specimen.

### 2.2. Observations of crack propagation and coalescence on the front of the specimen

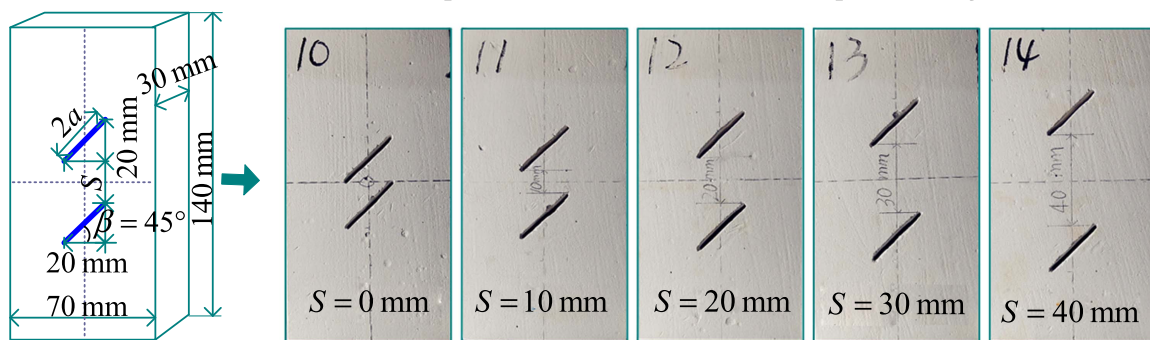
Surface crack patterns in solids play a significant role in determining the mechanical and physical properties of materials. Therefore, surface crack patterns are observed and recorded by the HD camera in the test. In figure 4, the surface patterns of crack propagation and coalescence on the specimen with different ratios of flaw depth to thickness ( $d/t$ , referred as flaw depth ratio) are presented. The crack patterns are classified into three types: wing cracks (the cracks initiate at the flaw tips and propagate along a curvilinear direction that becomes roughly parallel to the far field compression), secondary cracks (the cracks initiate at the flaw tips and propagate in a stable manner, and the extended direction and stress level of initiation are determined by the direction and magnitude of maximum shear) and coalescence cracks (the cracks that connect two pre-existing flaws). It should be noted that coalescence between two pre-existing flaws could be produced by wing cracks or secondary cracks or mixed wing and secondary cracks.

In figure 4(a), the flaw depth ratio  $d/t$  is  $1/3$ . On specimen 0# there are two wing cracks (① and ⑤) and wing crack (⑤) starts from the flaw tip and terminates at the lower flaw. On specimen 3# there are also two wing cracks, as well as on specimen 4#. In contrast, there are three secondary cracks on the specimen 0# surface, two secondary cracks on the specimen 3# surface and three secondary cracks on the specimen 4# surface. In addition, there was no crack occurrence around the pre-existing flaw tips in specimens 1# and 2#.

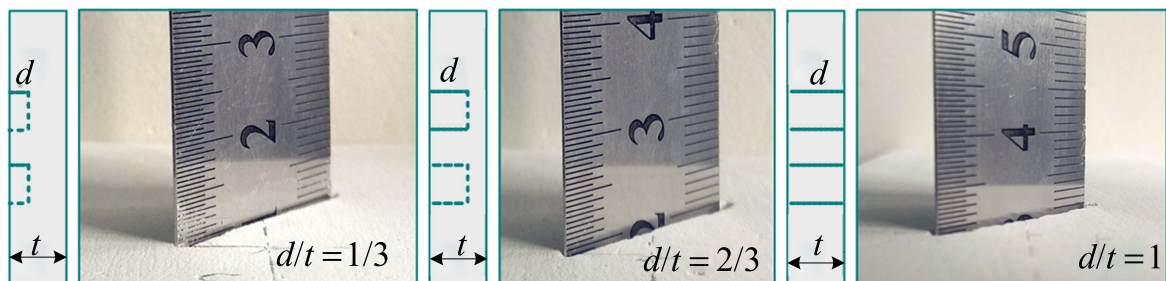
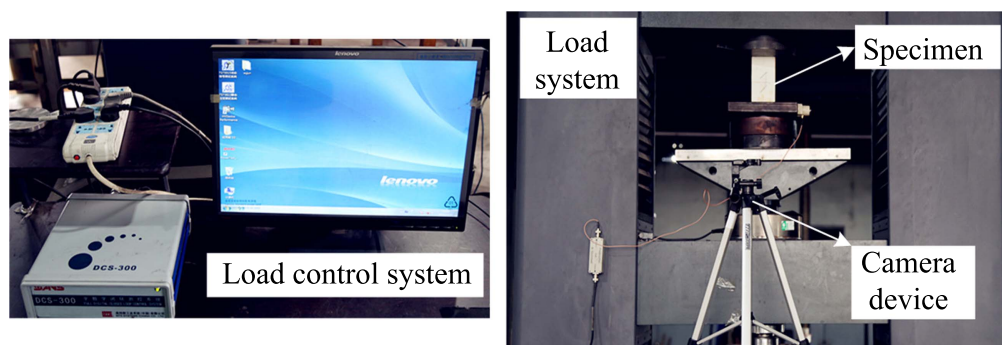
The surface patterns of crack propagation and coalescence are shown in figure 4(b) for when the flaw depth ratio is  $2/3$ . There are more surface cracks than for the results with the flaw depth ratio of  $1/3$ , however, the number decreases with increasing spacing between the flaws. In figure 4(c), where the flaw depth ratio is  $1$ , two clear wing cracks generated from flaw tips could be seen on each specimen, and the



(a) Mould for the specimen and sheet metal for the pre-existing flaw



(b) Geometry of the test specimens and flaws

(c) The ratios of flaw depth ( $d$ ) to thickness ( $t$ ) of the specimens**Figure 2.** Gypsum specimens in a uniaxial compression test.**Figure 3.** Experimental set up for the uniaxial compression test.



**Table 1.** Schemes of the uniaxial compression test.

| $d/t$ | Spacing/mm |     |     |     |     |
|-------|------------|-----|-----|-----|-----|
|       | 0          | 10  | 20  | 30  | 40  |
| 1/3   | 0#         | 1#  | 2#  | 3#  | 4#  |
| 2/3   | 5#         | 6#  | 7#  | 8#  | 9#  |
| 1     | 10#        | 11# | 12# | 13# | 14# |

number of coalescence cracks is more than the two conditions (ratios are 1/3 and 2/3) above.

### 3. The behaviour of crack propagation and coalescence

In this section, the behaviour of the crack propagation and coalescence due to the surface penetrating and non-penetrating flaws in the specimens under compression are classified and analysed based on the test results.

#### 3.1. Crack patterns of wing and secondary cracks on the front of specimens

In section 2.2, surface crack patterns are recorded and presented. According to the test results, the crack patterns are classified and summarized in table 2. In this section, the crack patterns of the wing and secondary cracks are analysed and the patterns of coalescence are discussed.

Wing cracks usually initiate at the tips of the pre-existing flaws and propagate in a nonlinear way towards the direction of loading compression, as presented and described in table 3 (Type I). There are two similar types of wing cracks in our tests. Wing crack Type I is common in experimental and numerical tests, and Type II could also be found in some experimental studies (Park and Bobet 2009, Cao et al 2015) and numerical investigations (Wong and Li 2013). In addition, the wing cracks presented in table 3 all occur in the situation of penetration. Therefore, it should be noted that the Type II wing crack can also occur when the pre-existing flaws are non-penetrating, such as wing crack ① in specimen 0#.

Secondary cracks initiate at the tips of pre-existing flaws and have been recognized by many researchers (e.g., Shen 1995, Bobet and Einstein 1998a, 1998b, Bobet 2000) as shear cracks. In compression, secondary cracks propagate in a stable manner, but the direction of propagation is random, and two directions are possible: (1) coplanar or nearly coplanar to the flaw and (2) in the opposite direction of the wing crack (Bobet 2000). From the specimen surface, the patterns of wing cracks are relatively smooth whereas the patterns of secondary cracks are sinuous and have many kinks, as shown in figure 4. Similar patterns of secondary cracks on the specimen surface can be found in many experimental investigations (e.g., Lajtai 1971, 1974, Shen 1995, Bobet and Einstein 1998a, Haeri et al 2014a, 2014b) or numerical simulations (e.g., Bobet and Einstein 1998b, Liang et al 2012, Wong and Li 2013).

Moreover, in the stage of crack propagation, some cracks keep growing while some cracks stop propagating in the failure progress due to the propagation of nearby cracks, such as wing cracks ① and ② in specimen 8#, secondary crack ⑤ in specimen 14# and coalescence crack ⑨ in specimen 5#.

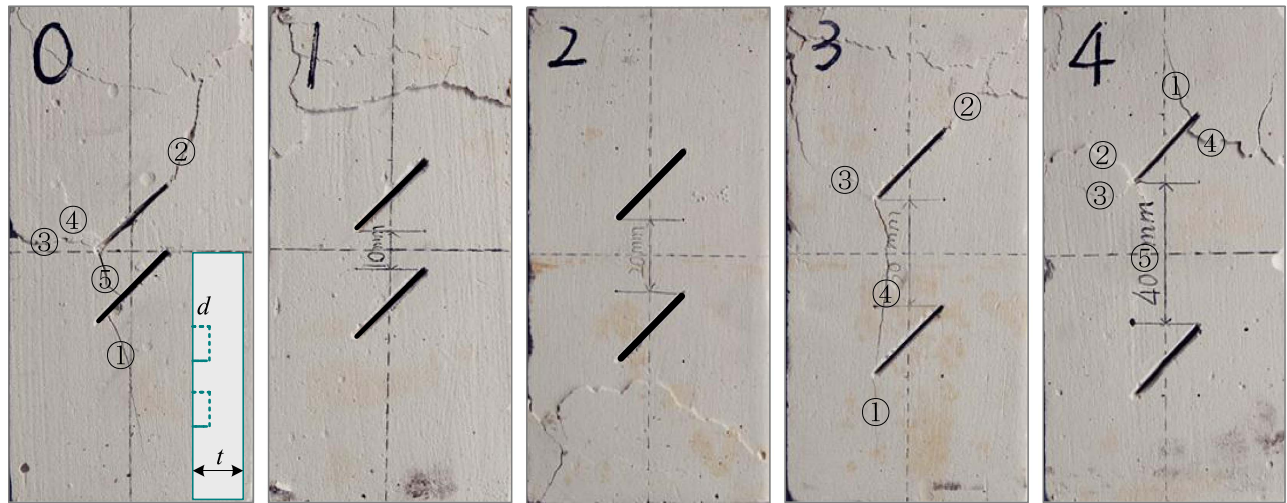
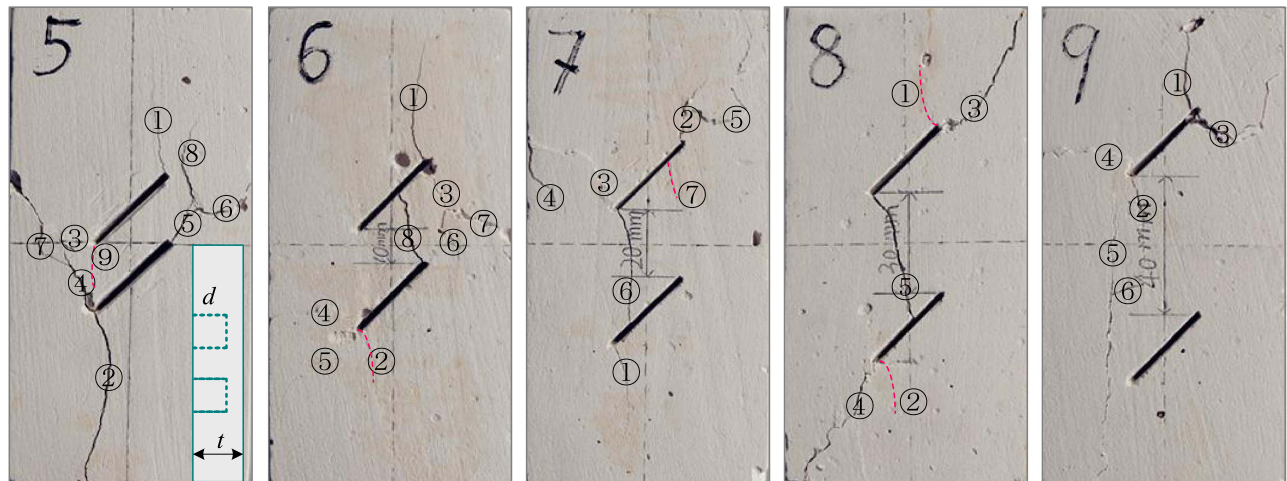
#### 3.2. Crack patterns of coalescence cracks on the fronts of specimens

Crack propagation and coalescence are the main reasons for cracked solid failures. The behaviour of coalescence cracks is significant for predicting the unstable failure of rocks. In table 4, four types of crack coalescence patterns are summarized and classified, and the detailed descriptions of these patterns are illustrated. From table 4, it can be seen that the spacing between the two pre-existing flaws plays an important role in the initiation and propagation of coalescence cracks. When the spacing is greater than 10 mm, the coalescence cracks are wing cracks in many cases, and there is usually one coalescence crack connecting the two pre-existing flaws. However, coalescence cracks extend as secondary cracks when the spacing is equal to or smaller than 10 mm. Actually, in some cases, it may also be wing cracks when the pre-existing flaw has a shallow depth, such as the coalescence crack in the specimen 0#.

According to the aforementioned observations and analyses, the overall patterns of crack growth are similar for penetrating and non-penetrating flaws. This means the crack patterns on specimen surfaces are similar in two-dimensional and three-dimensional conditions, as was also observed in the numerical investigations by Liang et al (2011, 2012). However, from the inside views (as shown in figure 5) of specimens and previous investigations (Dyskin et al 1999, 2003, Huang and Wong 2007, Liang et al 2012, Yin et al 2014) we know there are essential distinctions between two-dimensional and three-dimensional failure. For flaws that penetrate or are on the specimen surface, the coalescence of two pre-existing flaws usually occurs by linkage through wing cracks, secondary cracks or mixed wing and secondary cracks, but in non-penetrating flaws, the situation is variable and complex, which can be seen from figure 5. The surfaces of coalescence between dual non-penetrating surface flaws inside the specimen are uneven and rugged. Therefore, more experimental tests on non-penetrating flaws in rocks are needed for theoretical and numerical studies in future work.

### 4. The effect of the flaw depth ratio and spacing on specimen strength and crack propagation

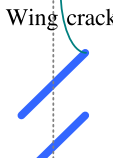
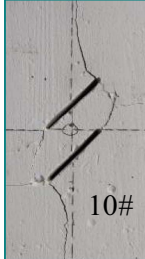
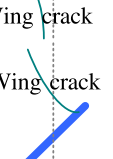
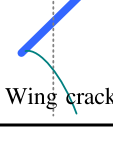

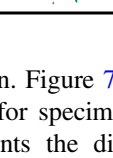
According to section 3, different crack patterns and surface characteristics in specimens with pre-existing flaws are presented and analysed. It could be seen that the flaw depth and spacing have a complex effect on the crack patterns. In this section, the effects of the flaw depth ratio and spacing on specimen strength and crack propagation are discussed. Figure 6 shows the load–displacement curves for all the specimens containing the same flaw depth ratio and different

(a) Surface crack features of specimens 0# ~ 4#,  $d/t = 1/3$ (b) Surface crack features of specimens 5# ~ 9#,  $d/t = 2/3$ (c) Surface crack features of specimens 10# ~ 14#,  $d/t = 1$ **Figure 4.** Surface crack features on specimens with different ratios of flaw depth and thickness.

**Table 2.** The classification of cracks on the specimens.

| Specimen | Wing crack | Secondary crack | Coalescence crack | Remarks                   |
|----------|------------|-----------------|-------------------|---------------------------|
| 0#       | ①⑤         | ②③④             | ⑤                 | —                         |
| 1#       | —          | —               | —                 | —                         |
| 2#       | —          | —               | —                 | —                         |
| 3#       | ①④         | ②③              | ④                 | —                         |
| 4#       | ①⑤         | ②③④             | ⑤                 | —                         |
| 5#       | ①②         | ③④⑤⑥⑦⑧⑨         | ⑨                 | ⑨ has been closed.        |
| 6#       | ①②⑧        | ③④⑤⑥⑦           | ⑧                 | ② has been closed.        |
| 7#       | ①⑥⑦        | ②③④⑤            | ⑥⑦                | ⑦ has been closed.        |
| 8#       | ①②⑤        | ③④              | ⑤                 | ① and ② have been closed. |
| 9#       | ①②         | ③④⑤⑥            | —                 | —                         |
| 10#      | ①②         | ③④⑤⑥⑦           | ⑥⑦                | —                         |
| 11#      | ①②⑥        | ③④⑤             | ⑤⑥                | —                         |
| 12#      | ①②⑤⑥       | ③④              | ⑤⑥                | ⑤ has been closed.        |
| 13#      | ①②⑥        | ③④⑤             | ⑥                 | ① has been closed.        |
| 14#      | ①②⑥        | ③④⑤             | ⑥                 | ① and ② have been closed. |

**Table 3.** Two similar types of wing crack patterns in the specimens.

| Type | Schematic path of wing cracks   | Description of wing cracks   |
|------|---|--|
| I    |   | <br>10#  |
|      |  |  |
| II   |  | <br>11# |
|      |  |  |

spacings under compression. Figure 7 shows the distribution of peak load (PL) values for specimens with different spacings, and figure 8 presents the distribution of the ratio between the residual load (RL) and PL for all the specimens under compression.

#### 4.1. Strength of the specimens with different flaw depth ratio and spacing

According to figure 6, the strength of the specimen could be influenced by the flaw depth ratio and spacing, especially when the flaw depth ratio is 1/3. The sensitivity could also be observed in figure 7, where the variances of the PL values for the two conditions with flaw depth ratios of 1/3 and 2/3 are 3.114 and 2.154, respectively. The variance of PL values decreases as the flaw depth increases. The sensitivity indicates that crack initiation can be affected by flaw depth and

spacing. When the flaw ratio  $d/t$  is equal to 1/3, partial failure occurs on the top and bottom of the specimens, and they show a failure pattern with some ductile features, though most of the load–displacement curves still possess a quasi-brittle pattern. However, such ductility disappears when the ratio is equal to 2/3 or 1. More cracks initiate at or near the pre-existing flaw tips as the ratio becomes larger than 1/3, as shown in figure 4. This result is similar to the studies of Wong *et al* (2004a, 2004b) on a single flaw suggesting that the critical flaw depth ratio is 0.3 for PMMA (about  $-50^\circ\text{C}$ ) and 0.1 for marble, which are both hard brittle solids.

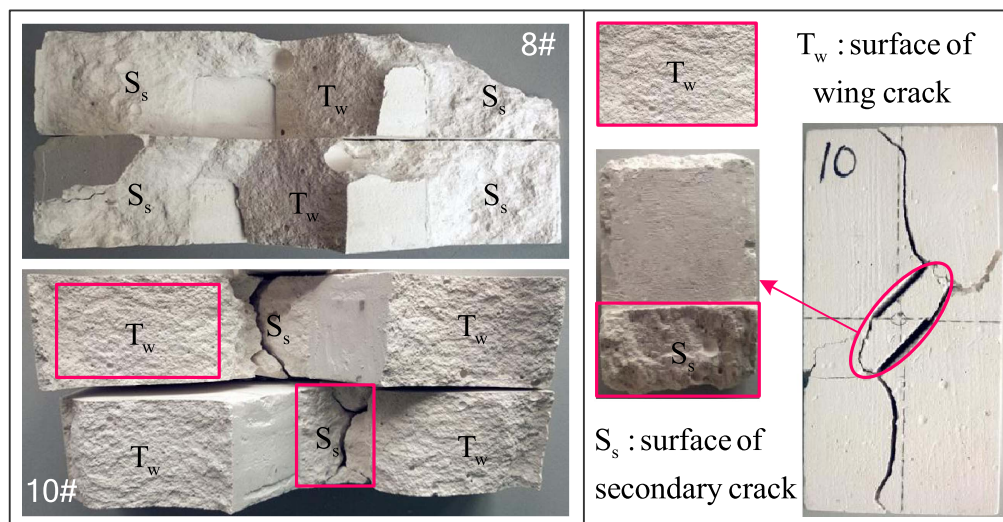
When the flaw depth ratio is 1, the variance of the PL values is only 0.398 indicating a lessening of the effect of spacing on strength for fully penetrating flaws. In this condition, the spacing mainly influences the crack patterns, as stated in the last section. In addition, as presented in figures 6



**Table 4.** Four types of coalescence crack patterns on surfaces of the specimens.

| Type | Schematic path of coalescence cracks |  |  |  | Description of coalescence  |
|------|--------------------------------------|--|--|--|---|
| I    |                                      |  |  |  | Coalescence model :Shearing,Tension<br>Characterization : Linkage is produced by two secondary cracks, or one wing crack and one secondary crack, or two wing cracks.   |
|      |                                      |  |  |  |   |
|      |                                      |  |  |  |   |
|      |                                      |  |  |  |   |
| II   |                                      |  |  |  | Coalescence model :Tension<br>Characterization : Linkage is produced by one smooth wing crack, which initiates at the upper flaw tip and propagates to the lower flaw, and the wing crack locates in the left part of the specimen. |
|      |                                      |  |  |  |   |
|      |                                      |  |  |  |   |
|      |                                      |  |  |  |   |
| III  |                                      |  |  |  | Coalescence model :Tension<br>Characterization : Linkage is produced by one wing crack, which initiates at the upper flaw tip and propagates to the middle or tip of the lower flaw.  |
|      |                                      |  |  |  |   |
|      |                                      |  |  |  |   |
|      |                                      |  |  |  |   |
| IV   |                                      |  |  |  | Coalescence model :Tension<br>Characterization : Linkage is produced by two wing cracks, and all of them locate in the right part of the specimen.  |
|      |                                      |  |  |  |   |
|      |                                      |  |  |  |   |
|      |                                      |  |  |  |   |

T : Tension  
S:Shearing

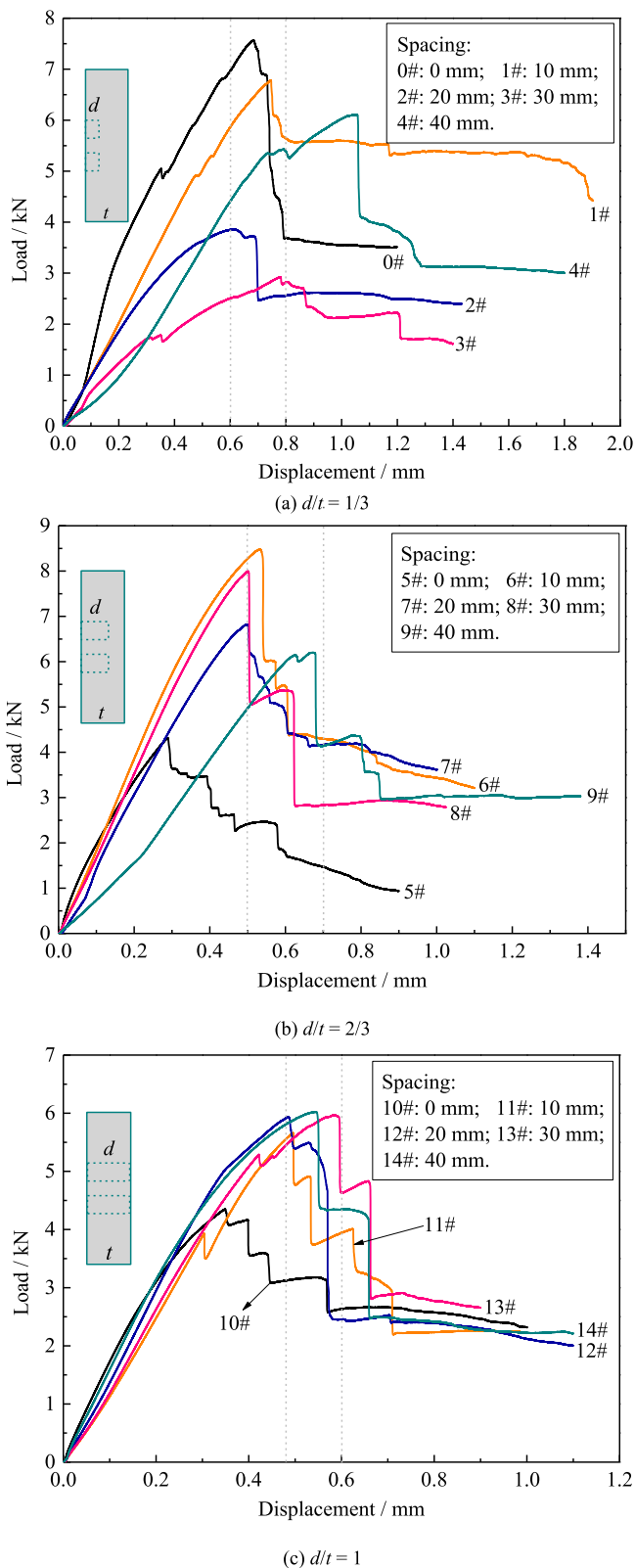
**Figure 5.** Surfaces of wing and secondary cracks in specimens 8# and 10#. The surface of the secondary crack is uneven and rugged whereas the surface of the wing crack is relatively smooth and flat.

and 7, the critical displacement corresponding to the peak specimen load has different ranges with respect to the flaw depth ratio. These critical displacements range from 0.6 to 0.8, 0.5 to 0.7 and 0.48 to 0.6, respectively, and, in general, are smaller as the flaw depth ratio increases.

#### 4.2. Stepped decline of the load–displacement curve

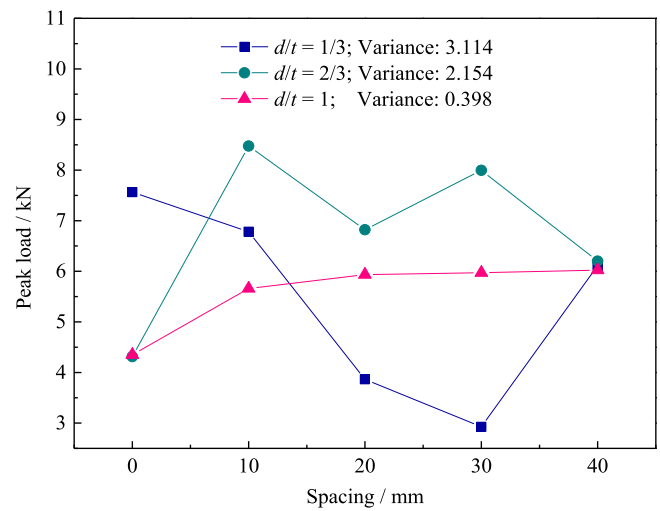
In figure 6, after the PL, an interesting note is the obvious stepped decline of the load value. According to the observations recorded by camera, the ‘stairs’ (stepped declines) occur



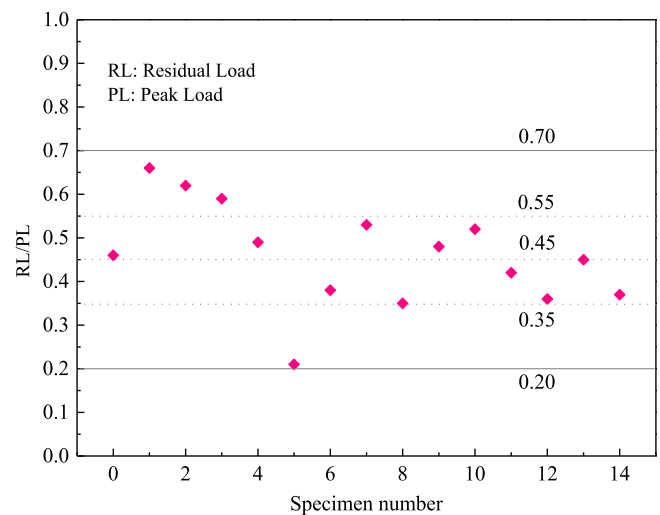


**Figure 6.** Load–displacement curves of the specimens with same flaw depth and different spacings.

with the generation of cracks, especially secondary cracks. Moreover, the ‘stairs’ in the load–displacement curves coincide with the development of shear cracks. This phenomenon indicates that crack propagation in the failure process is not



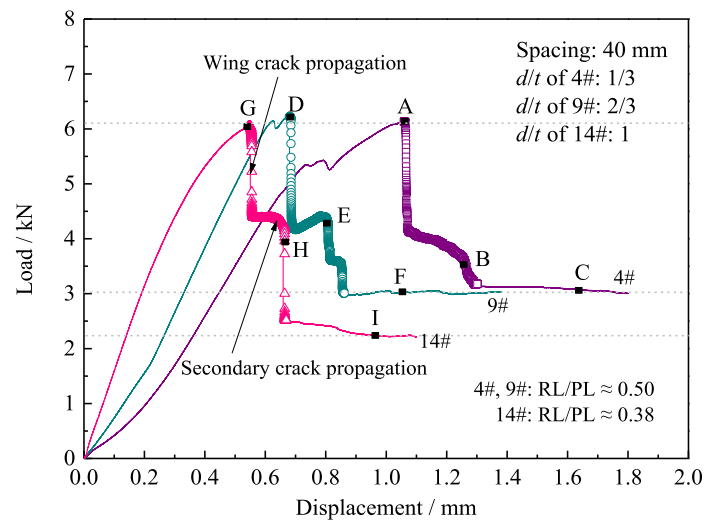
**Figure 7.** Peak load distribution of specimens.



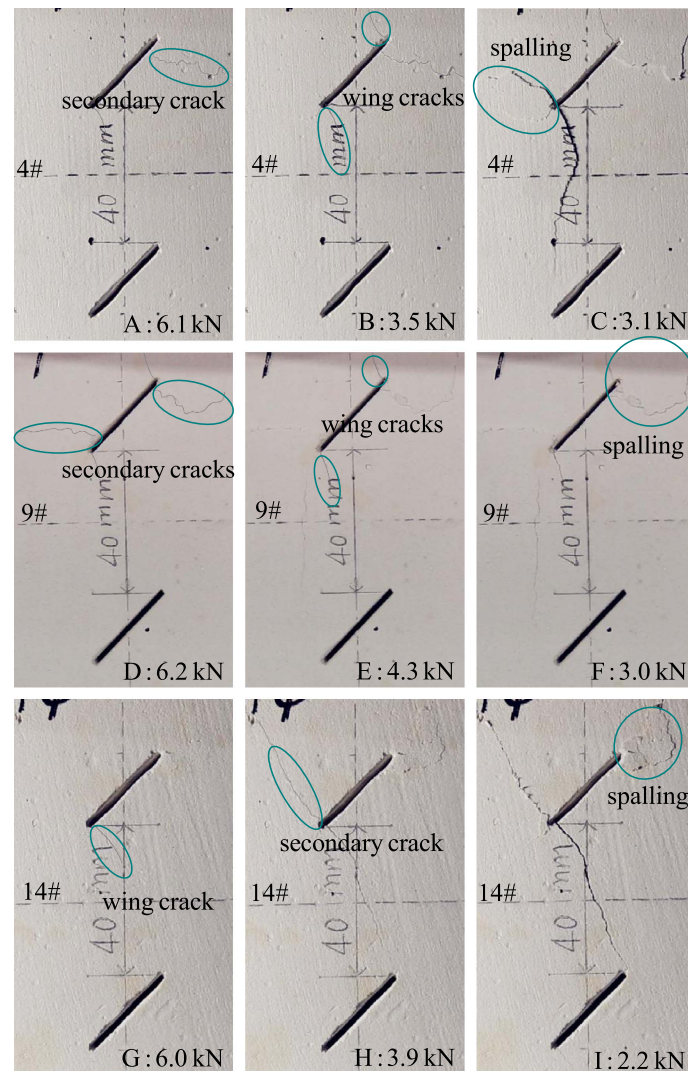
**Figure 8.** RL/PL distribution of the specimens in uniaxial compression.

always continuous, and the secondary cracks initiate and propagate one by one unlike the initiation and propagation of wing cracks before the PL or at the PL. This phenomenon could also be interpreted as that more secondary cracks are generated and propagate in the condition of deep flaw depth.

Furthermore, in order to highlight and analyse the relationship between the RL and PL of the specimen, the ratio RL/PL is calculated and plotted in figure 8 with the specimen number. It was found that the values of RL/PL for the specimens 0# ~ 4# ( $d/t = 1/3$ ) are all larger than 0.45 and smaller than 0.70. Apart from specimen 5# with the lowest RL/PL ratio. When the flaw depth ratio is 2/3, for specimens 6# ~ 9#, the values of RL/PL fluctuate approximately 0.45 as the spacing changes. In specimens 11# ~ 14# (flaw depth ratio is 1), the values of RL/PL range from 0.35 to 0.45, and the influence of spacing is reduced. According to the results, we find that the value of RL/PL at failure has a tendency to decrease with the increase of flaw depth.

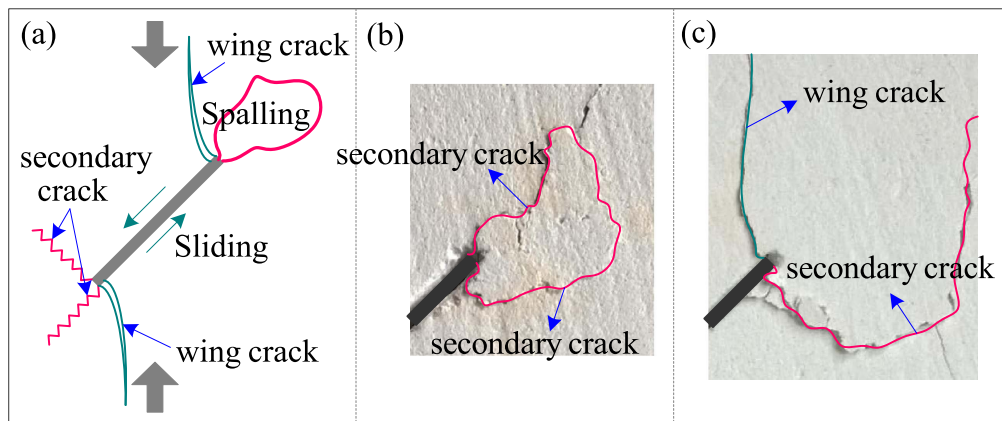


(a) Load-displacement curves of specimens 4#, 9# and 14#



(b) Crack propagation at various stages of load for the three specimens

**Figure 9.** Load–displacement curves and surface crack propagation for specimens 4#, 9# and 14#.



**Figure 10.** Diagrammatic sketch of crack propagation and two possible types of spalling formation. Spalling in diagram (b) is caused by secondary cracks, and spalling in diagram (c) is caused by secondary and wing cracks.

### 5. The effect of crack propagation and coalescence on specimen residual strength

In this section, specimen residual strength is investigated based on the crack propagation and coalescence, and some phenomena observed in the test are also investigated and discussed based on the test results.

Figure 9(a) shows the load–displacement curves and figure 9(b) shows surface crack propagation during the loading process for specimens 4#, 9# and 14#. These results were chosen to compare the effect of the flaw depth ratio and flaw separation on crack propagation, load–displacement curves, and strength. It can be seen that the PL values of the specimens are not particularly sensitive to the flaw depth ratio when the spacing is 40 mm. From figure 8 we see that the ratio of RL/PL of specimen 4#, as well as specimen 9#, is 0.50, which is 0.12 higher than the ratio of RL/PL for specimen 14#. In specimens 4# and 9# wing cracks initiate before the PL and secondary cracks occur at the PL, but on the surface of specimen 14#, wing cracks occur at the PL. In addition, with crack initiation and propagation, the curve of the load fluctuates (curves of specimens 4# and 9#), and the load value has a relatively large amplitude decline after the PL (specimen 14#). Additionally, the rate of decline caused by wing crack propagation is faster than the rate of decline caused by secondary crack propagation.

In addition, the phenomenon of spalling (failure of a portion of the surface caused by coalescence of cracks) occurs, which could be regarded as an indication of specimen failure. Once spalling initiates failure of the specimen quickly comes to an end. In figure 9(b) the spalling is mostly caused by the propagation and coalescence of secondary cracks according to the patterns on the specimen surface. They indicate that the flaw depth ratio or spacing could affect spalling by dominating the initiation and propagation of secondary cracks. Indirectly, wing cracks also play an important role in the process of spalling formation, such as in specimens 4# or 9#.

In addition, some previous investigations (Bobet and Einstein 1998a, Wong and Einstein 2009a, Park and Bobet 2010) have also reported that spalling is closely related

to the propagation and coalescence of secondary cracks. Therefore, we may gain two possible types of spalling formation: (1) spalling is caused by secondary cracks; and (2) spalling is caused by secondary and wing cracks, as shown in figures 10(b) and (c).

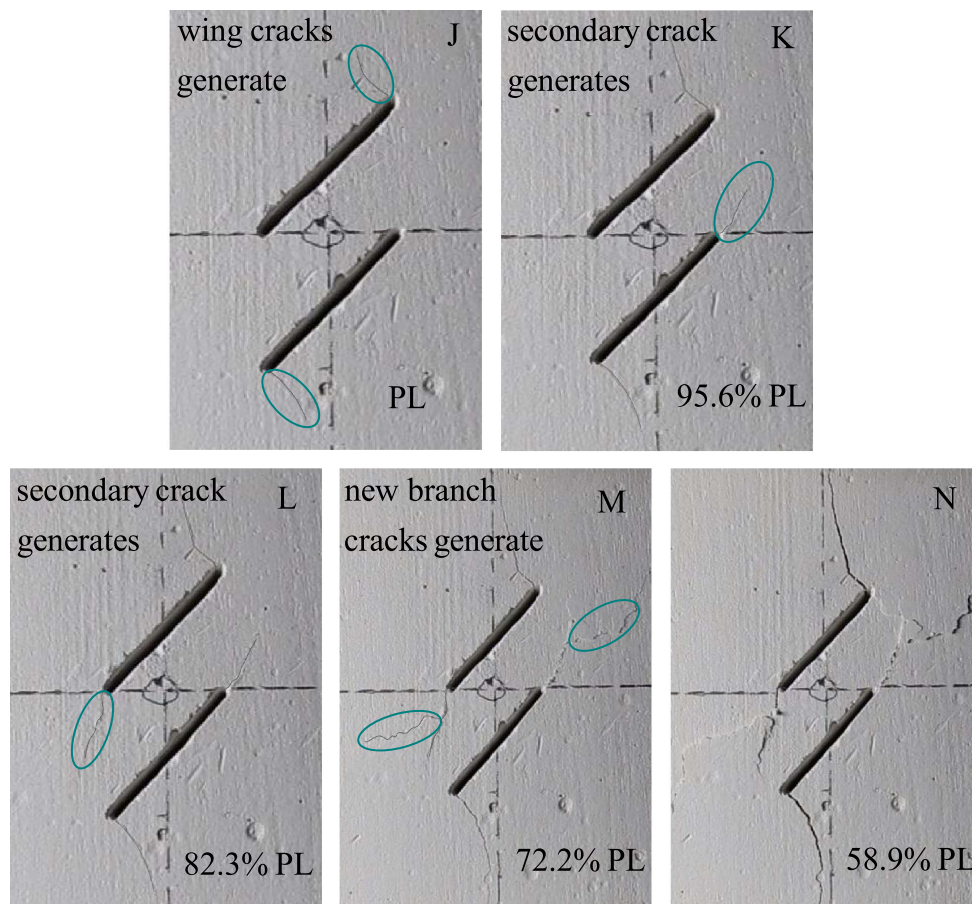
Figure 11 shows the crack propagation process on the surface of specimen 10#. After PL, the short wing cracks initiate and begin to propagate in a stable manner along a curvilinear path from point J to point K. At points K and L, secondary cracks occur one by one, and the load value decreases simultaneously. Then, both the secondary and wing cracks continue to propagate with further compression. At point M, crack branching occurs on the secondary cracks, roughly coincident with the decline of load value acceleration. Moreover, according to the results, the load level when the wing crack occurs is higher by approximately 4.4% than that of secondary crack generation on the surface of specimen 10#. The stepped decline of the load value could be clearly found in figure 11(b). Compared with specimens 11# ~ 14# with larger spacing, there are more decline steps in the curve of specimen 10#.

### 6. Conclusions

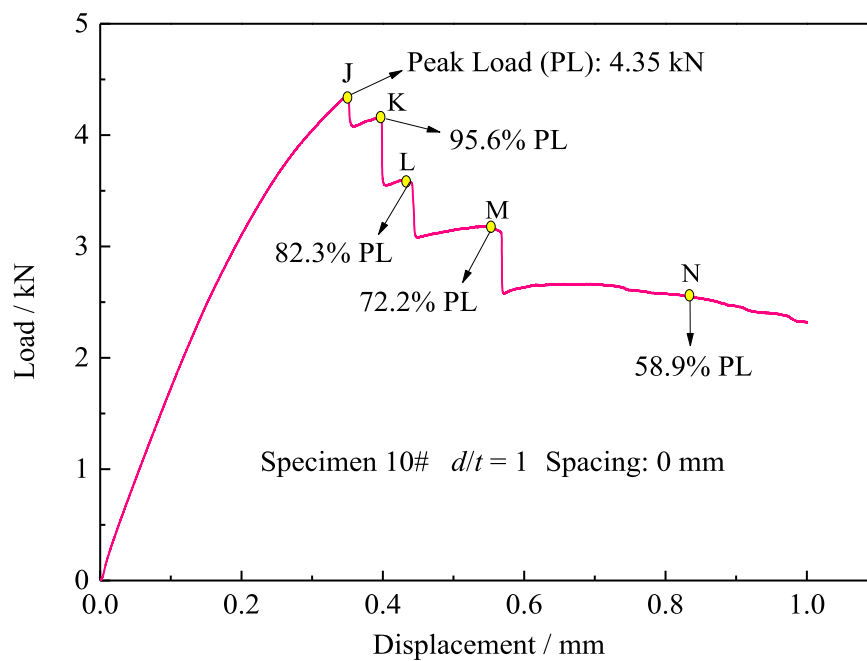
Gypsum specimens with dual non-penetrating and penetrating flaws were used to investigate the surface crack behaviour and strength of soft rock material under compression by considering crack propagation and coalescence, the flaw depth ratio, and the spacing between the flaws. The results show that the flaw depth ratio and spacing have an influence on the crack initiation, propagation, and coalescence and their effect on the strength of the specimen. Based on the test results, the following conclusions could be reached:

1. Wing cracks in soft brittle material are similar to those in other hard brittle material (e.g., granite and ceramics). Two similar types of wing cracks are observed, and four types of coalescence crack paths on the specimen surface are also detected and clarified.





(a) Surface crack propagation after peak load for specimen 10#



(b) Load-displacement curve of specimen 10#

**Figure 11.** Surface crack propagation and load–displacement curve for specimen 10# under compression.

2. Under compression, surface crack patterns could be influenced directly by the flaw depth ratio and the spacing between the flaws. Few cracks emanate from the pre-existing flaws when the flaw depth ratio is equal to 1/3, and more cracks occur with the increase of the flaw depth ratio. A larger flaw depth ratio could advance the occurrence of the PL and result in a smaller residual strength after failure. More secondary cracks occur when a smaller spacing exists between the dual flaws. In addition, the number of cracks also increases when the flaw depth ratio increases.
3. When the pre-existing dual flaws are non-penetrating, the strength of the specimen and crack propagation are sensitive to the flaw depth ratio and spacing between the flaws. If the pre-existing dual flaws are penetrating, the spacing has a low impact on specimen strength, and in this case, the spacing mainly influences the crack patterns. In addition, the crack propagation and coalescence could influence the specimen residual strength. A larger flaw depth ratio could promote specimen brittleness and result in a smaller specimen residual strength.
4. The RL/PL ratio of the specimen with non-penetrating flaws is larger than for penetrating flaws. In addition, spalling usually occurs because of the propagation and coalescence of secondary cracks, which could be regarded as indicating when the crack goes into the final stage of propagation. That means once spalling initiates failure of the specimen quickly comes to an end. Moreover, two possible types of spalling formation are briefly discussed.

## Acknowledgments

The work described in this paper was substantially supported by the National Program on Major Research Project (No. 2016YFC0701301-02) and Jiangsu Higher Education Institutions for the Priority Academic Development Program (CE02-1-34), both of them are gratefully acknowledged.

## References

- Adams M and Sines G 1978 Crack extension from flaws in a brittle material subjected to compression *Tectonophysics* **49** 97–118
- Ashby M F and Hallam S D 1986 The failure of brittle solids containing small cracks under compressive stress states *Acta Metall.* **34** 497–510
- Bi J, Zhou X P and Qian Q H 2016 The 3D numerical simulation for the propagation process of multiple pre-existing flaws in rock-like materials subjected to biaxial compressive loads *Rock Mech. Rock Eng.* **49** 1611–27
- Bobet A 2000 The initiation of secondary cracks in compression *Eng. Fract. Mech.* **66** 187–219
- Bobet A and Einstein H H 1998a Fracture coalescence in rock-type materials under uniaxial and biaxial compression *Int. J. Rock Mech. Min. Sci.* **35** 863–88
- Bobet A and Einstein H H 1998b Numerical modeling of fracture coalescence in a model rock material *Int. J. Fract.* **92** 221–52
- Brace W F and Bombolakis E G 1963 A note on brittle crack growth in compression *J. Geophys. Res.* **68** 3709–13
- Cao P, Liu T Y, Pu C Z and Lin H 2015 Crack propagation and coalescence of brittle rock-like specimens with pre-existing cracks in compression *Eng. Geol.* **187** 113–21
- Dyskin A V, Germanovich L N and Ustinov K B 1999 A 3D model of wing crack growth and interaction *Eng. Fract. Mech.* **63** 81–110
- Dyskin A V, Sahouryeh E, Jewell R J and Ustinov K B 2003 Influence of shape and locations of initial 3D cracks on their growth in uniaxial compression *Eng. Fract. Mech.* **70** 2115–36
- Feng X T, Ding W X and Zhang D X 2009 Multi-crack interaction in limestone subject to stress and flow of chemical solutions *Int. J. Rock Mech. Min. Sci.* **46** 159–71
- Haeri H, Shahriar K, Marji M F and Moarefvand P 2014a On the strength and crack propagation process of the pre-cracked rock-like specimens under uniaxial compression *Strength Mater.* **46** 140–52
- Haeri H, Shahriar K, Marji M F and Moarefvand P 2014b Investigation of fracturing process of rock-like Brazilian disks containing three parallel cracks under compressive line loading *Strength Mater.* **46** 404–16
- Haeri H, Shahriar K, Marji M F and Moarefvand P 2014c Experimental and numerical study of crack propagation and coalescence in pre-cracked rock-like disks *Int. J. Rock Mech. Min. Sci.* **67** 20–8
- Haeri H, Shahriar K, Marji M F and Moarefvand P 2015a On the HDD analysis of micro crack initiation, propagation and coalescence in brittle materials *Arab. J. Geosci.* **8** 2841–52
- Haeri H, Shahriar K, Marji M F and Moarefvand P 2015b A coupled numerical-experimental study of the breakage process of brittle substances *Arab. J. Geosci.* **8** 809–25
- Hoek E and Bieniawski Z T 1965 Brittle fracture propagation in rock under compression *Int. J. Fract. Mech.* **1** 137–55
- Huang J F, Chen G G, Zhao Y G and Wang R 1990 An experimental study of the strain field development prior to failure of a marble plate under compression *Tectonophysics* **175** 269–84
- Huang M L and Wong R H C 2007 Experimental study on propagation and coalescence mechanisms of 3D surface cracks *Chin. J. Rock Mech. Eng.* **26** 1794–9 (in Chinese)
- Ingraffea A R and Heuze F E 1980 Finite element models for rock fracture mechanics *Int. J. Numer. Anal. Methods Geomech.* **4** 25–43
- Lajtai E Z 1971 A theoretical and experimental evaluation of the Griffith theory of brittle fracture *Tectonophysics* **11** 129–56
- Lajtai E Z 1974 Brittle fracture in compression *Int. J. Fract.* **10** 525–36
- Lee H and Jeon S 2011 An experimental and numerical study of fracture coalescence in pre-cracked specimens under uniaxial compression *Int. J. Solids Struct.* **48** 979–99
- Li Y P, Chen L Z and Wang Y H 2005 Experimental research on pre-cracked marble under compression *Int. J. Solids Struct.* **42** 2505–16
- Liang Z Z, Li L C, Tang S B and Zhang Y B 2011 3D numerical simulation of growth of surface crack of rock specimens *Chin. J. Geotech. Eng.* **33** 1615–22 (in Chinese)
- Liang Z Z, Xing H, Wang S Y, Williams D J and Tang C A 2012 A three-dimensional numerical investigation of the fracture of rock specimens containing a pre-existing surface flaw *Comput. Geotech.* **45** 19–33
- Morgen S P, Johnson C A and Einstein H H 2013 Cracking processes in Barre granite: fracture process zones and crack coalescence *Int. J. Fract.* **180** 177–204

- Mughieda O and Alzo'ubi A K 2004 Fracture mechanisms of offset rock joints—a laboratory investigation *Geotech. Geol. Eng.* **22** 545–62
- Park C H and Bobet A 2009 Crack coalescence in specimens with open and closed flaws: a comparison *Int. J. Rock Mech. Min. Sci.* **46** 819–29
- Park C H and Bobet A 2010 Crack initiation, propagation and coalescence from frictional flaws in uniaxial compression *Eng. Fract. Mech.* **77** 2727–48
- Reyes O and Einstein H H 1991 Failure mechanism of fractured rock—a fracture coalescence model *Proc. 7th Int. Congress on Rock Mechanics, (Aachen)* pp 333–40
- Sagong M and Bobet A 2002 Coalescence of multiple flaws in a rock-model material in uniaxial compression *Int. J. Rock Mech. Min. Sci.* **39** 229–41
- Schulson E M, Kuehn G A, Jones D A and Fifolt D A 1991 The growth of wing cracks and the brittle compressive failure of ice *Acta Metall. Mater.* **39** 2651–5
- Shen B 1995 The mechanism of fracture coalescence in compression—experimental study and numerical simulation *Eng. Fract. Mech.* **51** 73–85
- Shen B and Stephansson O 1993 Numerical analysis of mixed mode I and mode II fracture propagation *Int. J. Rock Mech. Min. Sci. Geomech. Abstr.* **30** 861–7
- Tang C A, Lin P, Wong R H C and Chau K T 2001 Analysis of crack coalescence in rock-like materials containing three flaws: II. Numerical approach *Int. J. Rock Mech. Min. Sci.* **38** 925–39
- Teng C K, Yin X C, Li S Y and Cai D E 1987 Experimental study of three dimensional fracture in plate specimens with non-penetrating crack *Acta Geophys. Sinica* **30** 371–8 (in Chinese)
- Vekinis G, Ashby M F and Beaumont P W R 1993 Plaster of Paris as a model material for brittle porous solids *J. Mater. Sci.* **28** 3221–7
- Wong L N Y and Einstein H H 2009a Crack coalescence in molded gypsum and Carrara marble: I. Macroscopic observations and interpretation *Rock Mech. Rock Eng.* **42** 475–511
- Wong L N Y and Einstein H H 2009b Crack coalescence in molded gypsum and Carrara marble: II. Microscopic observations and interpretation *Rock Mech. Rock Eng.* **42** 513–45
- Wong L N Y and Li H Q 2013 Numerical study on coalescence of two pre-existing coplanar flaws in rock *Int. J. Solids Struct.* **50** 3685–706
- Wong R H C and Chau K T 1998 Crack coalescence in a rock-like material containing two cracks *Int. J. Rock Mech. Min. Sci.* **35** 147–64
- Wong R H C, Chau K T, Tang C A and Lin P 2001 Analysis of crack coalescence in rock-like materials containing three flaws: I. Experimental approach *Int. J. Rock Mech. Min. Sci.* **38** 909–24
- Wong R H C, Guo Y S H, Chau K T, Zhu W S and Li S C 2007 The crack growth mechanism from 3-D surface flaw with strain and acoustic emission measurement under axial compression *Key Eng. Mater.* **353–8** 2357–360
- Wong R H C, Huang M L, Jiao M R, Tang C A and Zhu W 2004a The mechanisms of crack propagation from 3D fracture under uniaxial compression *Key Eng. Mater.* **261–263** 219–24
- Wong R H C, Law C M, Chau K T and Zhu W 2004b Crack propagation from 3D surface fractures in PMMA and marble specimens under uniaxial compression *Int. J. Rock Mech. Min. Sci.* **41** 37–42
- Yang S Q 2011 Crack coalescence behavior of brittle sandstone samples containing two coplanar fissures in the process of deformation failure *Eng. Fract. Mech.* **78** 3059–81
- Yang S Y and Jing H W 2011 Strength failure and crack coalescence behavior of brittle sandstone samples containing a single fissure under uniaxial compression *Int. J. Fract.* **168** 227–50
- Yang S Y, Liu X R and Jing H W 2013 Experimental investigation on fracture coalescence behavior of red sandstone containing two unparallel fissures under uniaxial compression *Int. J. Rock Mech. Min. Sci.* **63** 82–92
- Yin P, Wong R H C and Chau K T 2014 Coalescence of two parallel pre-existing surface cracks in granite *Int. J. Rock Mech. Min. Sci.* **68** 66–84
- Zhou X P, Cheng H and Feng Y F 2014 An experimental study of crack coalescence behavior in rock-like materials containing multiple flaws under uniaxial compression *Rock Mech. Rock Eng.* **47** 1961–86
- Zhou X P and Yang H Q 2012 Multiscale numerical modeling of propagation and coalescence of multiple cracks in rock masses *Int. J. Rock Mech. Min. Sci.* **55** 15–27